An experimental investigation of fracture processes in glass-ceramic sealant by means of acoustic emission

Rangel-Hernandez V.H.[a,b,1], Fang Q.[a], Babelot C.[c], Lohoff R.[c], and Blum L.[a]

[a]*Institute of Electrochemical Process Engineering (IEK-14), Forschungszentrum Jülich GmbH, 52425 Jülich, Germany.*

[b]*Department of Mechanical Engineering, Engineering Division, University of Guanajuato, Salamanca, Gto., México C.P. 36885.*

[c]*Central Institute of Engineering, Electronics and Analytics (ZEA-1), Forschungszentrum Jülich GmbH, 52425. Jülich, Germany.*

Abstract

One of the essential components for ensuring the long service life of solid oxide cell (SOC) stacks is the sealant used. Therefore, in this work, an experimental investigation of the glass ceramic sealant (GCS) fracture process was carried out using an Acoustic Emission (AE) based approach. A series of tensile tests at room temperature were performed and the acoustic activity emitted was recorded by two AE sensors. An AE signal analysis was then performed using two approaches: wave mode identification and frequency content analysis. To understand the fracture process of the GCS, the analysis was supported with prior knowledge of the GCS microstructure and a post-test visual analysis. This demonstrated the presence of low-frequency failure mechanisms (50-400 kHz) such as debonding, fiber pull-out and matrix cracking, and high-frequency mechanisms (> 400 kHz) such as fiber breakage. The results confirm the suitability of using the acoustic emission approach for monitoring failure events and show its potential application in SOC stacks monitoring.

---

[1] Corresponding author
Email address: v.rangel-hernandez@fz-juelich.de
vrangel@ugto.mx

Keywords: Acoustic emission (AE), damage mechanisms, glass-ceramic, fast Fourier transform (FFT), AE energy.

1. Introduction

Today, the global race for sustainable energy and industrial decarbonisation has greatly boosted the scaling up of hydrogen technologies [1]. In this respect, the solid oxide cell (SOC) is considered a promising technology, as its potential to generate and store power in highly efficient and sustainable way has been widely shown [2]. In particular, the planar solid oxide cell (SOC) stack consists of a top plate and a bottom plate, ceramic cells, metallic interconnectors and contact materials on the anode and cathode sides. In addition, it requires the use of a sealing material, made of glass ceramic that entraps the gases inside the stack and also functions as an electrical insulator [3]. This diversity of materials and the fact that in operation an SOC stack is subjected to significant thermal gradients results in the generation of important mechanical stresses due to the different thermal expansion coefficients of the materials and its deformation [4, 5]. As a result, the sealants may fracture, preventing the optimal operation of the SOC stack. Due to the adverse environment in which they operate, the direct inspection and/or monitoring of the sealants using current electrochemical techniques such as electrochemical impedance spectroscopy (EIS) is practically impossible [6].

For this reason, the glass ceramic sealant (GCS) has been the subject of several developments and research has focused on improving its thermomechanical behavior in different operating conditions [7-9]. In this respect, Wei et al. [10] characterized the mechanical behavior of sealants under tensile and bending strengths at room temperature. Smeacetto et al. [11] studied the chemical and thermo-mechanical compatibility of a proposed glass ceramic sealant, based on a sodium-calcium-alumino-silicate glass ceramic, with Crofer22APU and yttria-stabilized-zirconia (YSZ) and found an excellent performance of the sealant in the experiments. Goel et al. [12] investigated the influence of Bi_2O_3 addition on the sintering and crystallization behavior, flow properties of diopside ($CaMgSi_2O_6$) based glass ceramics. According to the results, the glass-ceramic turned out to be a potential sealant for applications in SOFC stacks. Malzbender et al. [13] characterized the mechanical behavior, fracture and creep of different sealant materials subjected to both room and high temperatures. On the other hand, Gross et al. [14] improved the mechanical properties of sealants by adding fillers as reinforcements.

More recently, Zhang et al. [15] proposed a novel Al_2O_3-glass composite as sealant for use in SOFC stack and the results demonstrated an excellent thermo-mechanical performance

Likewise, Timurkutluk et al. [16] demonstrated the thermos-mechanical reliability of different types and configurations of ceramic glass sealants through tensile and short stack leakage tests. Other studies on this subject have also been reported in recent years [17-20].

However, there are few reports in literature on understanding the formation and propagation of fractures in the glass-ceramic sealant used in SOC stacks. Hence, the interest in the use of non-destructive techniques (NDTs) to monitor and evaluate their mechanical degradation has increased. NDT is a technique that has been widely used for several years in engineering fields such as civil [21, 22], aeronautical and space [23, 24], geothermal [25, 26] and material engineering [27, 28]. However, only a few works has been undertaken to evaluate the mechanical degradation of SOC stacks. In this way, Surgeon et al [29] studied the mechanical response, damage development and the AE activity of barium-magnesium aluminosilicate

(BMAS) glass-ceramic reinforced with Tyranno silicon carbide (SiC) subjected to tensile loadings. The results allowed the differentiation of different fracture mechanism such as matrix micro-cracking, matrix macro-cracking, interface debonding and delamination cracking. Jiayu Li et al. [30] applied an AE method for detecting the fracture process, as well as the onset condition for fracture damage in a single cell. A characterization of the emission pattern was provided, namely: pattern A (cathode vertical cracking), B (cathode delamination) and C (vertical cracking in the electrolyte), which exhibited predominant frequencies of about 130 kHz, 240 kHz and the widest frequencies, respectively. Similarly, Sato et al. [31] investigated the mechanical performance of solid oxide fuel cells in simulated environments using AE. Their findings also showed vertical cracking and delamination in the cathode, as well as vertical cracking in the electrolyte. On the other hand, Malzbender et al. [4] investigated the correlation between the occurrence of failure and the operating conditions of SOCs based on acoustic emission. The experiments were performed with multiple thermal heating-cooling loops, but no quantitative data was provided to implement a diagnostic system based on AE.

In view of the above, and as far as the authors are aware, no acoustic emission research has been conducted involving the type of glass ceramic sealant used here, and so the study poses a further challenge in identifying the sealant’s fracture mechanisms. Therefore, current experimental research seeks to provide initial knowledge for understanding the fracture process of this type of ceramic by means of the AE) approach. To this end, annular butt joint specimens entrapping glass-ceramic sealant in the radial and circumferential directions were subjected to tensile loadings in order to monitor and analyze the acoustic activity of the tests. The AE analysis was carried out using the Fast Fourier Transform (FFT) technique, thus calculating the frequency spectrum of the AE waves. Scanning electron microscopy and energy dispersive X-ray spectroscopy (SEM/EDS) was then used to elicit the microstructure and chemical composition of the glass-ceramic sealant and support the AE analysis. Finally, a post-test analysis of the fractured piece was carried out in order to corroborate the results and support the explanation of the fracture process.

2. Materials and testing methods

2.1 Specimens preparation

The standard ceramic glass material used as sealant in SOC stacks at Forschungszentrum Jülich GmbH is used in this work. It is a material composed of barium-calcium-silicate glass, a glass H and reinforced with 13 % wt. yttria-stabilized-zirconia fibers [32, 33]. The chemical composition of the glass H is provided in Table 1.The coefficient of thermal expansion (CTE) of the glass H is9.6 x 10^{-6} K^{-1} (from 200 °C to 600 °C) and the CTE for glass H reinforced with YSZ fibers is 9.3 x 10^{-6} K^{-1} (from 200 °C to 600 °C) [34].

Table 1. Chemical composition of glass H (in Wt. %) [33].

	BaO	SiO2	CaO	Additions
Wt. %	48.2	29.8	6.1	Al_2O_3, B_2O_3 V_2O_5, ZnO

Annular butt joint specimens, made of Crofer 22 APU, were prepared in accordance with the model suggested by Gross et al. [33]. The CTE for the Crofer22 APU is 11.4 x 10^{-6} K^{-1} (from 20°C to 600 °C). Therefore, the coefficient of thermal expansion of the Crofer 22 APU and the glass-ceramic sealant are compatible within the SOC stack . The glass-ceramic sealant was deposited radially and circumferentially on the surface of the butt joints with a 24 mm external radius and 12 mm internal radius. The specimens were thermally bonded at 850 C for 100 hours to crystallize the glass H and then cooled at a rate of 2 K/min (no flaws yielded during the cooling process), as is currently being conducted for the SOC-stacks operated at Forschungszentrum Jülich GmbH.

In addition, to ensure stable monitoring of the acoustic waves emitted by the fracturing of the material, each specimen was fitted with 70 mm long cylindrical waveguides. At one end of these, conical bases were fixed to position the AE sensors, as can be seen in Fig. 1.

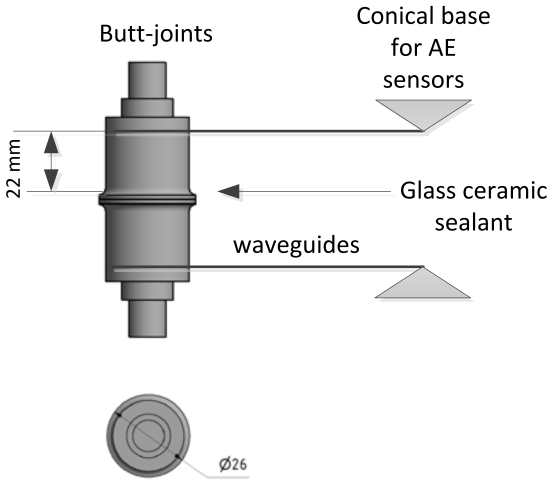

Fig. 1. Schematic of the annular butt joints used as specimens in the tensile tests measurements [33].

2.2. Tensile loading measurement

The tensile loading measurements were carried out on a pneumatic stress testing bench at room temperature, as is shown in Fig. 2. The specimens were mounted in the internal frame of the machine and held in place by fastening screws placed at both ends of the specimen. The AE sensors were mounted on the conical bases and fixed by a copper housing. Thus, each of the specimens was subjected to a tensile load applied at a rate of 0.5 mm/min. The acoustic activity emitted during testing was then recorded electronically in the AE equipment.

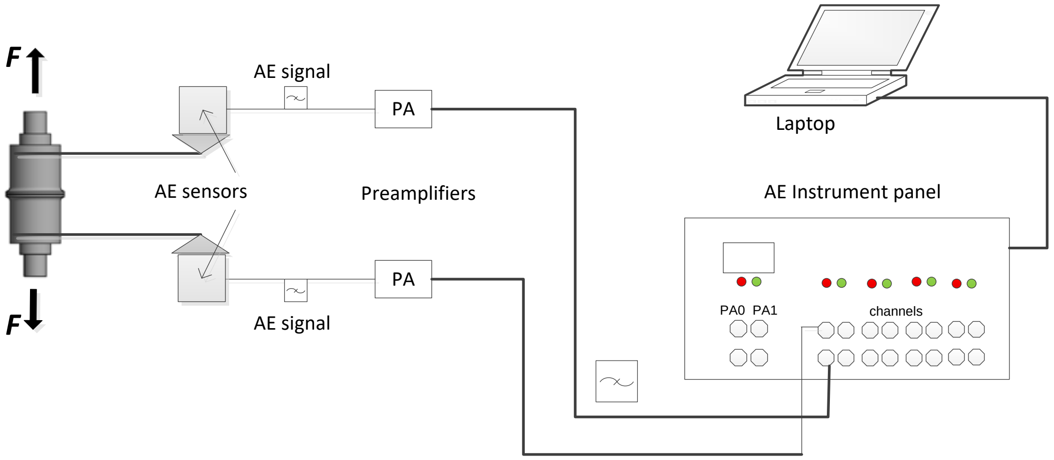

Fig. 2. Schematic of the AE sensors and cylindrical-shaped samples set-up for tensile tests.

2.3. AE monitoring equipment

The AE monitoring system included a set of AE sensors (VS160-NS) with a frequency range of between 100 and 450 kHz, a set of AE wide-band pre-amplifiers (AEP5H) with a gaining band of 40 dB at 50 ohms, as well as the AMSY-6 digital 12-channel AE Vallen measurement system (MB6-V1) equipped with four +/- 10 V parametric input channels to monitor the temperature. Real time data recording and post data management were performed on both Vallen Sysveri R2017 software [35] and Matlab [36]. The AE sample rate was set to 10 MHz and the TR (transient data) sample rate was set to 5 MHz. The noise from external sources was filtered by establishing a detection threshold of 40 dB in accordance with the results obtained in the characterization background noise test. The correct setting up of the AE sensors was then verified by the Hsu-Nielsen test [37].

2.4 Post-test analysis

In order to verify the fracture of the ceramic glass sealant, it was embedded in epoxy resin to be metallographically prepared. The cross-section of the samples were analyzed with Scanning Electron Microscopy (SEM) using ZEISS Sigma VP and the chemical composition was measured with energy-disperse X-ray spectroscopy (EDS, Oxford EDS X-maxN). Finally, the fracture surface of the failed specimens was physically and visually analyzed in order to find their relation with the fracture mechanisms found in the acoustic emission analysis.

3. Analysis of the results

3.1 Analysis of the AE measurements

The AE monitoring of the tensile loading of the specimen yielded 900 data containing continuous, transient and noise acoustic emission sources. Therefore, a signal discrimination routine based on signal duration was applied as suggested in [38]. As is shown in Fig. 3, it was possible to identify four clusters of data. First, signals falling within cluster I were characterized by low amplitude, long duration and continuous sources; signals located in cluster II were characterized by a spike and short duration signals, i.e. electromagnetically induced noise [39,40]; cluster III was mostly made up of transient signals that contained the important information to be analyzed; and, cluster IV was mainly characterized by saturated signals. It is of interest to note the change in slope between region I and region III, which indicates the transition between continuous and transient signals. In particular, the signals in region III arise from spontaneous release of energy during cracking and show a linear correlation [38, 41]. Accordingly, the criterion proposed here for filtering the data was to consider only those of burst type, i.e. signals from Cluster III and some from Cluster I that could satisfy the condition of an amplitude greater than 40 dB and a duration greater than 2000 μs.

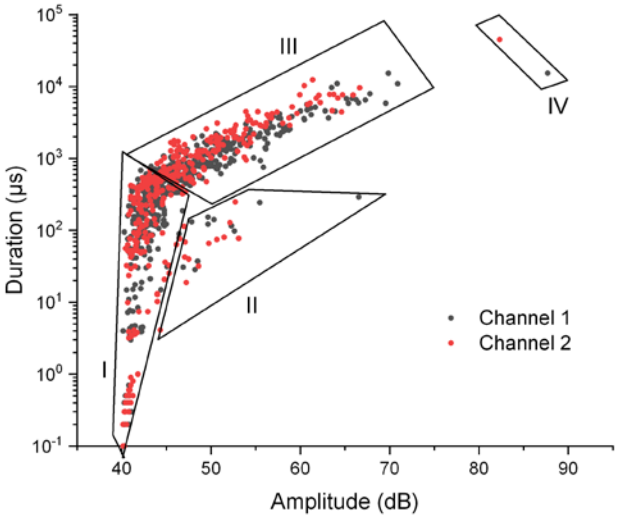

Fig. 3. Diagram of amplitude versus duration of acoustic emission signals from tensile loading, categorized in four regions I to IV, depending on the duration.

Fig. 4 displays the resulting correlation between the peak AE amplitude of events and the tensile force over time. Importantly, an event is represented by a pair of points (i.e. signals from channel 1 and channel 2). Based on this, it is clear that most of the acoustic activity collected during the application of the tensile load was kept below 70 dB, except for the event that coincided with the end of the test at 11 kN maximum load. However, this event showed data saturation, so was not suitable for analysis. A possible explanation for the low amplitudes could be inferred from the size of the crack or the speed of crack propagation. The highest concentration of activity coincides with the specimen's fracture point. The steep slope of the tensile curve can be attributed to the elastic crack propagation of internal flaws or cracks. Interestingly, there is clearly a region where the acoustic activity apparently ceases, between 200 and 230 s, which is probably due to a pore or defects saturation effect.

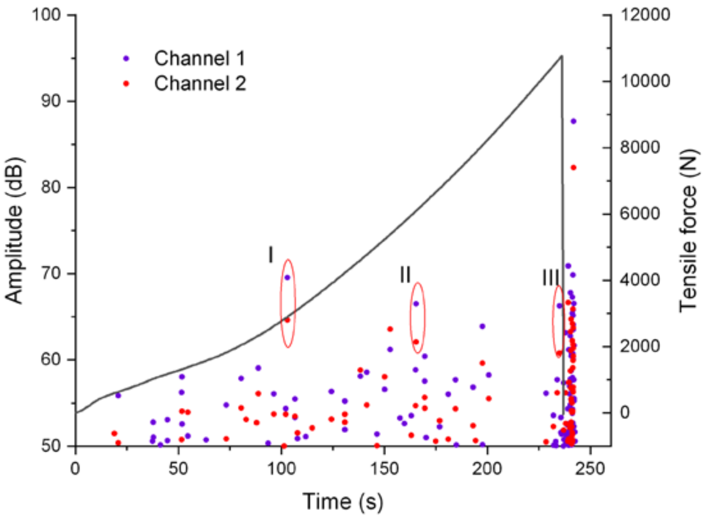

Fig. 4. AE correlation diagram of a representative specimen tested at room temperature and prepared with glass-ceramic sealant, showing the peak amplitude and tensile loading vs the testing time: events from channel 1 and channel 2.

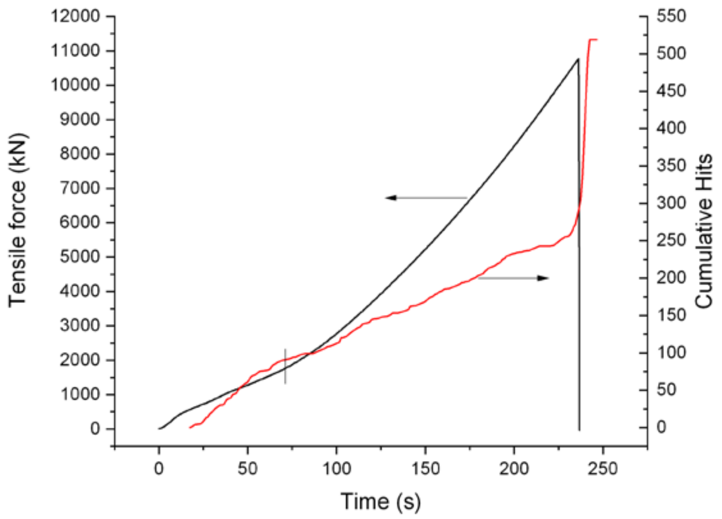

Fig. 5. Evolution of load and cumulative number of hits during tensile test of glass ceramic sealant.

Fig. 5 reveals the evolution of the tensile loading and cumulative number of AE hits as a function of time. The cumulative number of hits started rising sharply right after application of tensile load. However, immediately after the first change in the evolution of the load (i.e. first proportional limit at roughly 1800 kN), which is indicated on the plot, the damage to the glass ceramic sealant is slower. It is probable that the first cumulative hits are due to the appearing of micro-cracks in the matrix and then a combination of macro-cracks and fiber-matrix debonding or delamination. A hypothesis that is confirmed later. Noteworthy that there is a slight flattening of the cumulative hits curve just before the failure takes place. This flattening coincided with the region of apparent ceasing of acoustic activity observed earlier in Fig. 6. This finding is consistent with that of Surgeon et al. [29] who observed a saturation crack zone in some of the tensile experiments with BMAS glass-ceramic matrix reinforced with SiC fibers. The final failing of the glass-ceramic specimen triggered the cumulative hits.

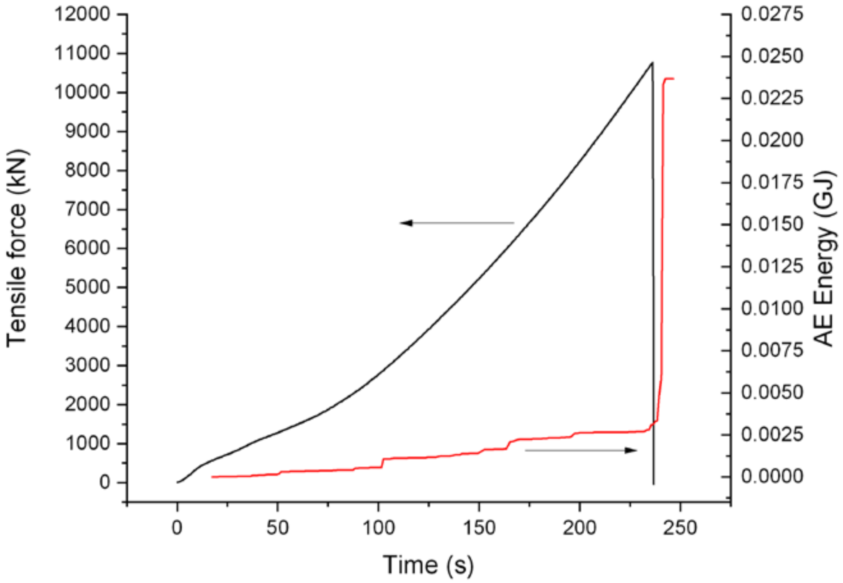

Fig. 6. Evolution of load and AE energy during tensile test of glass ceramic sealant.

The evolution of AE energy and the tensile force as a function of time are given in Fig. 6. The AE energy initiated to increase just after the first proportional limit. Interestingly there is also a flattening in the AE energy curve between 200 and 230 s, which coincides with the commented above. This finding may result from the fact that since there is no acoustic activity, there is no propagation of the energy wave. Similarly, the failing of the glass ceramic sealant triggered the Ae energy.

In order to explain the fracture process of the glass ceramic sealant under investigation, three representative cases are considered in the following analysis. For further reference, the three cases have been defined in Fig. 6 as events I, II and III and are enclosed in red.

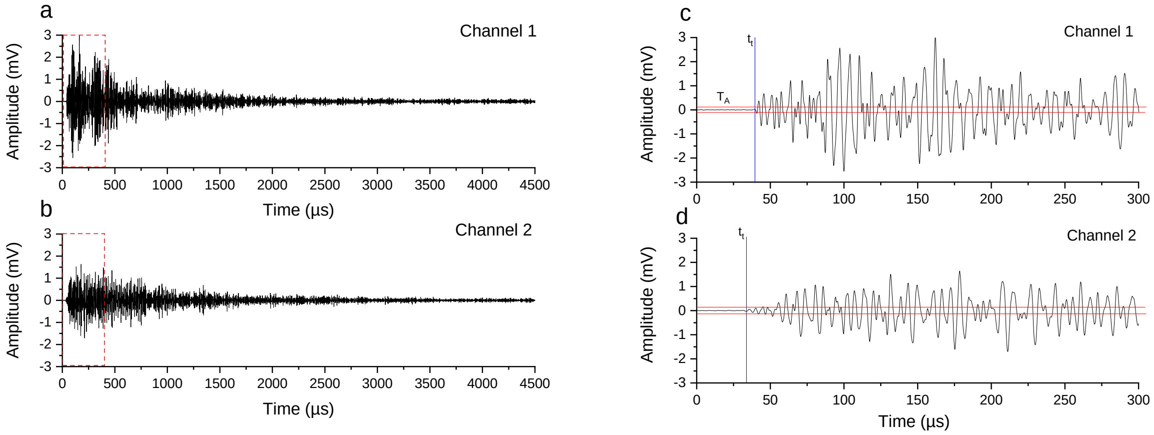

Fig. 7. AE signal obtained from channel 1 and 2 of event I: long view (a-b) and initial fragment of the signals (c-d).

Fig. 7 illustrates the signals obtained from event I during the tensile test: 100 seconds after the onset of the test. The long view from channel 1 (Fig. 7a) shows a signal of the transient type with several peaks of amplitude, the most representative being the burst that reaches 3 mV. In the case of channel 2 (Fig. 7b), the signal is also of the transient type but with a lower amplitude than the first one. The difference in amplitude in the signal pair is a clear evidence of the attenuation experienced by the signal on reaching channel 2. A probable explanation for this phenomenon may be the direction of the radiation from the emission source which may not be the same for both sides due to the geometry of the specimen.

In an attempt to relate the AE waveforms to a possible wave mode and, hence, to a fracture mechanism as suggested by many of the existing published studies [41-43], the signals are analyzed in detail as they appear in Fig. 7 (c-d). The solid vertical line indicates the trigger time, t_t; whereas the solid horizontal lines indicate threshold amplitude, T_A. In both cases the threshold was set at 0.1 mV (40 dB_{AE}). During the trigger time, a difference of 5 μs was clearly shown between the signal of channel 2 and that of channel 1. This difference may be attributed to the orientation of the AE source. By comparing these waveforms with the results of previous research based on wave modes analysis [41-43], it could be determined that there was no indication that these waveforms would be related to the fundamental guided wave modes. However, it was interesting to observe that these types of waveforms occurred in cases where the waveguide design generated a change in the wave propagation modes, which in this particular case was the rod wave mode, as was previously reported in [38].

As there were not enough elements to relate the previously reviewed wave modes to the fracture mechanisms, an FFT was performed on the signals. The frequency spectra of both signals are shown in Fig. 8. A visualization of the frequencies allows two frequency ranges to be distinguished, the first between 0 and 200 kHz, and the second ranges from 200 kHz to 400 kHz. However, there are some small peaks above 400 kHz that are outweighed by the other frequencies. For the example of channel 1, Fig. 8a, the frequency spectrum shows several peaks, the highest being 132 kHz. Then, in the next frequency range, the highest peak is 230 kHz. On the other hand, in the example of channel 2, Fig. 8b, the frequency peak in the first range was 170 kHz, while for the next range it was 240 kHz.

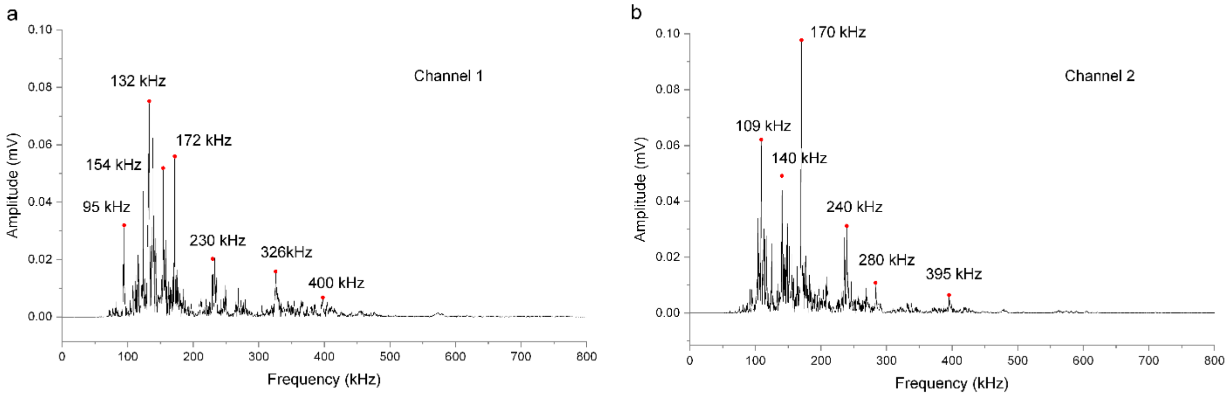

Fig. 8. Signal frequency spectrum of channel 1 (a) and channel 2 (b).

As suggested by various researchers [39, 44-46], and considering that in both examples the signals are dominated by low frequencies, it can be inferred from the above that these events can be attributed to the debonding and fiber pull-out mechanisms. For the glass ceramic sealant used here, the YSZ fibers are placed in the H glass perpendicular to the tensile force. Therefore, when the specimen is subjected to the tensile force, the fibers tend to separate from the H-glass (i.e. fiber pull-out), just as with the rest of the crystals, forming two fracture surfaces or cleavage planes in accordance with the theory of the fracture of ceramics [47, 48]. It is assumed that the onset of the crack was in one of the pores or in some defect of the glass ceramic sealant, as these are high stress concentration fields. As there is no evidence of high frequencies, it can be deduced that there was no breakage of YSZ fibers and, therefore, this event is only related to the fracture occurring between the glass H, the YSZ fibers and the crystals, i.e. debonding.

The second example, event II, contains a pair of signals with the AE waveforms shown in Fig. 9. The transient signal from channel 1 presents several peaks of amplitude, the highest one reaching nearly 2 mV, in Fig. 9a. The signal from channel 2, on the other hand, has amplitude peaks almost half of those shown in the signal of channel 1, Fig. 9b. This difference in amplitude may be due, as explained above, to the speed of cracking or crack size.

As for the wave mode analysis, it can be seen that in this particular case, the trigger times were similar, at 40 μs, on the basis of which it can be assumed that radiation from the source was similar towards both sensors. In this context, the waveforms do not present features that relate them to the wave modes established for thin plates [30]. However, as explained above, the wave modes osberved in both cases fall within the classificaction of the rod mode.

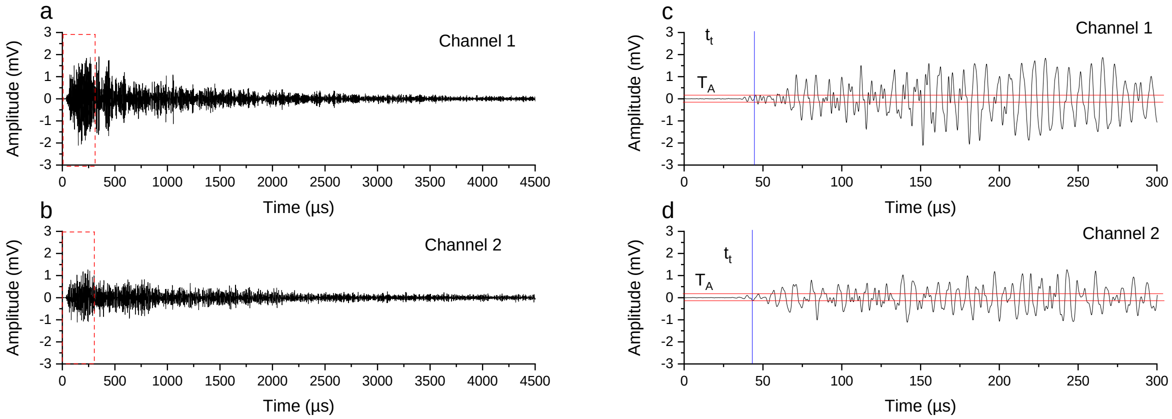

Fig. 9. AE signal obtained from channel 1 and 2 of event II: long view (a-b) and initial fragment of the signals (c-d).

The frequency content of the signal pair is shown in Fig. 10. The analysis uses the classification of the frequency range defined above, i.e. 0 to 200 kHz and 200 to 400 kHz.

Accordingly, channel 1 has a low-frequency peak of 134 kHz, while channel 2 has a peak of 170 kHz. In the high frequency range, on the other hand, the frequency peak coincides in the pair of spectra, 242 kHz. However, in both signals the low frequency predominates, which can be attributed to delamination and fiber pull-out mechanisms.

Furthermore, some traces of higher frequency can be seen, 411 kHz in the case of channel 1, which can be attributed to fiber cracking, but due to its low magnitude does not interfere with the predominant low frequency values.

.

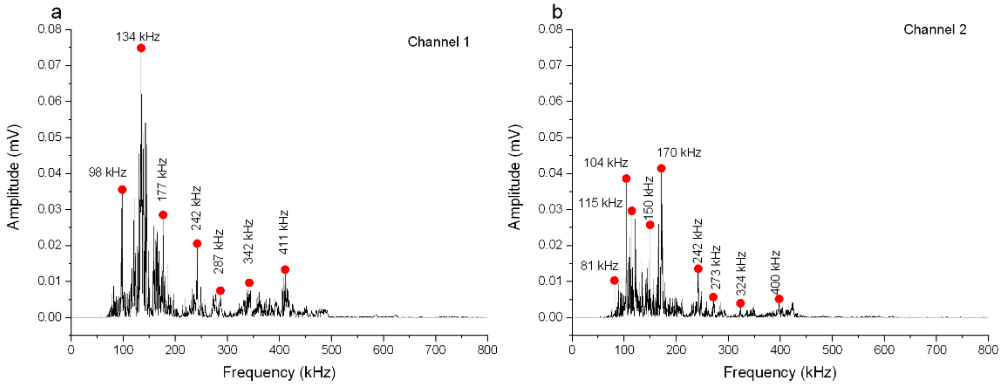

Fig. 10. Signal frequency spectrum of channel 1 (a) and channel 2 (b).

Further illustration of the identification of the fracture mechanisms can be given using the signals from event III, Fig. 11. The AE waveforms of the signal from channel 1 (Fig. 11a) and channel 2 (Fig. 11b) show quite interesting behavior. In both cases, the trigger time occurred later than in previous ones, in which it was almost immediate. A possible explanation for this event may be the position of the emission source with respect to that of the sensors or the path taken by the signal towards them.

In this case, the wave mode analysis also did not make it possible to determine whether there were fundamental wave modes for the plates. Therefore, as in the cases analyzed above, the wave mode observed here was the rod mode.

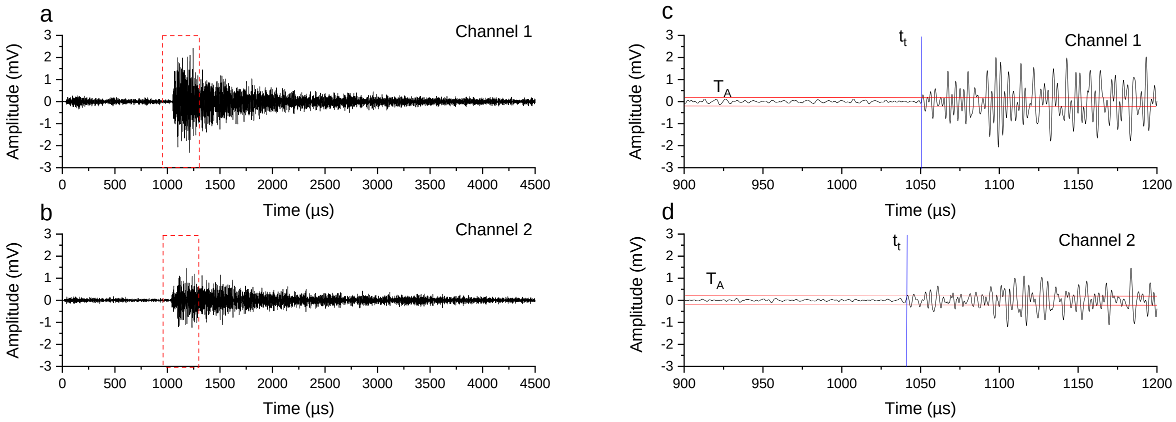

Fig. 11. AE signal obtained from channel 1 and 2 of event III: long view (a-b) and initial fragment of the signals (c-d).

The frequency spectra for the two analyzed signals are shown in Fig. 12. This reveals a frequency peak in the low frequency range of 170 kHz, and then a peak at 335 kHz in the second frequency range, but also significant frequency peaks above 400 kHz. In the example of channel 2, Fig. 12b, there is also a frequency peak at 170 kHz in the first range of frequency and 235 kHz in the second range of the frequency.

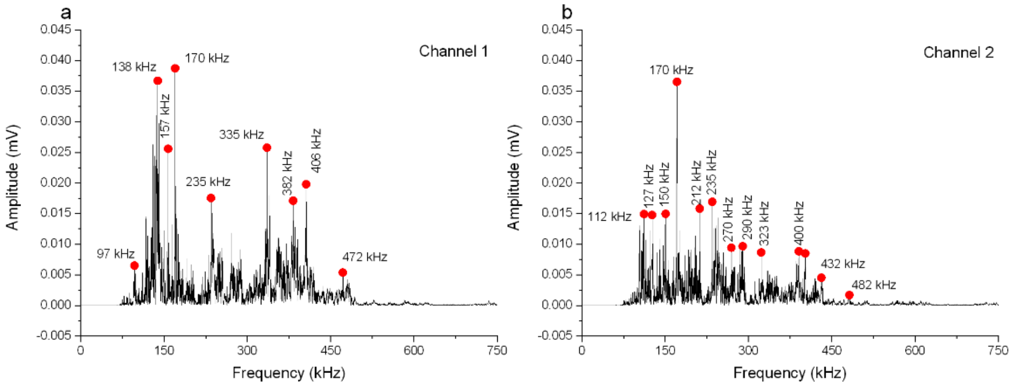

Fig. 12. Signal frequency spectrum of channel 1 (a) and channel 2 (b).

Above these, there appear to be significant frequency peaks such as 482 kHz, and some between 500 and 700 kHz. These latter frequencies did not occur previously, which suggests another fracture mechanism such as fiber breakage [39, 44-46]. Yet, when considering the specific structure of the glass ceramic sealant considered here, these high frequencies may be attributed to either YSZ-fibers breakage or crystals breakage.

3.2 Post-test analysis

The analysis of the microstructure and chemical composition of the glass-ceramic sealant was performed after the tests by means of scanning electron microscopy and X-ray diffraction (SEM/EDS). The combination of both methods enabled the identification of several crystalline phases after the joining, as already studied by Brendt et al. [49]. Fig. 13 (a) reveals the microstructure of the sealant (glass H) on SEM images, with and EDS-analysis in Fig. 13 (b). Accordingly, the following chemical elements were found: zinc, silicon, aluminum, yttrium, zirconium, barium, calcium and oxygen. All phases detected are oxides: (Ba, Si) oxide, (Ba, Si, Ca) oxide, (Ba, Si, Al) oxide and YSZ. According to [49], the silicate phases correspond to two different barium silicates ($Ba_2Si_3O_8$ and $Ba_5Si_8O_9$), celsian ($BaAl_2Si_2O_8$) and walstromite ($BaCa_2Si_3O_9$), as confirmed by the X-ray diffraction measurement. After 100 hours at 850 °C the glass H was not completely crystallized and a residual glass phase was observed as well as some pores. Fig. 14 shows EDS-measurements of silicon, zirconium, aluminum and calcium. This made it possible to better distinguish the different crystalline phases in the image, in particular the needle-like form of the (Ba, Si, Al) oxide phase. In addition, the comparison of silicon and zirconium pointed to the interaction between the YSZ-fibers and glass H, as well as the appearance of zirconate at the edges.

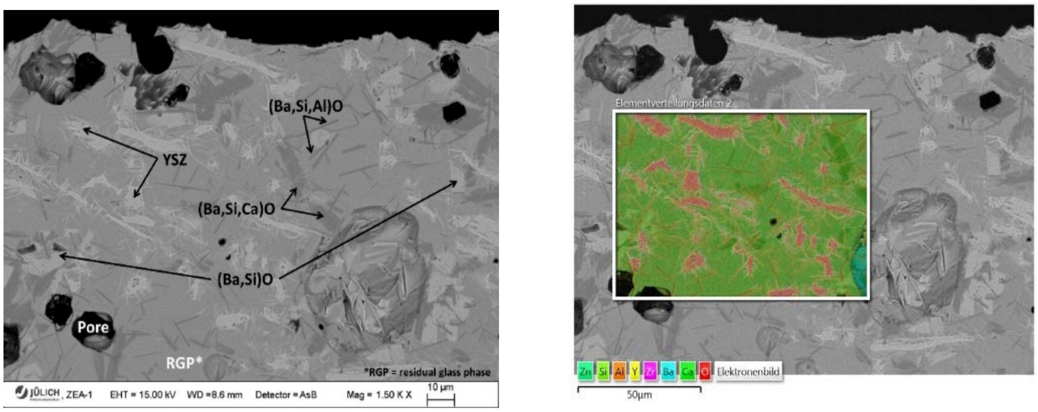

Fig. 13: a) SEM-image of glass-ceramic sealant composed of glass H enriched with YSZ-fibers and b) EDS-analysis of a sample taken from the SEM-picture

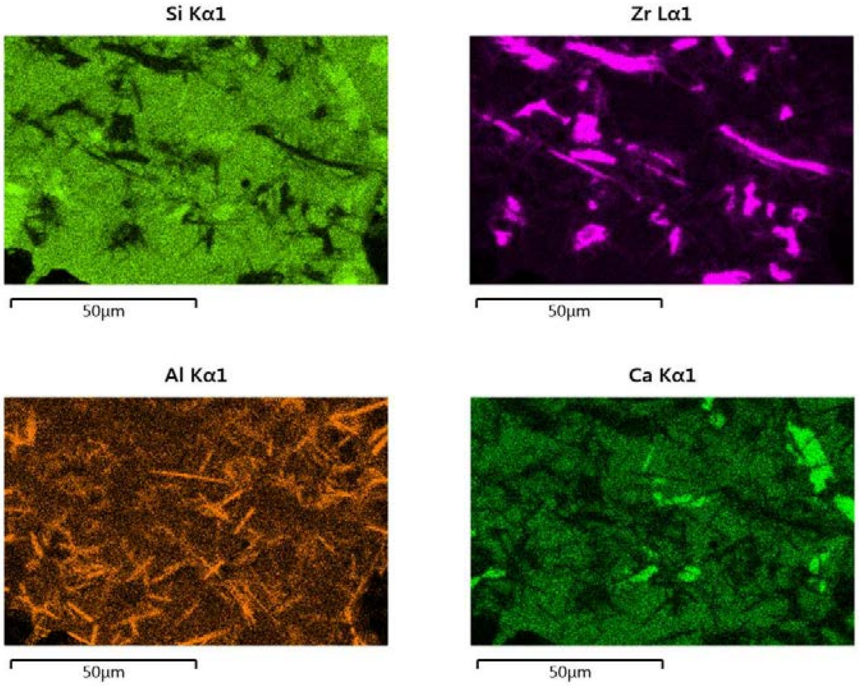

Fig. 14: EDS-measurement of silicon, zirconium, aluminum and calcium, four components of glass H enriched with YSZ.

.In order to complement and verify what was analyzed previously, it was proceeded to visually review one of the pieces, Fig. 15. The seams seen on the inner and outer part of the specimen were created during the bonding process, their main component is barium chromate, and are formed on the three-phase steel/glass/air boundary.

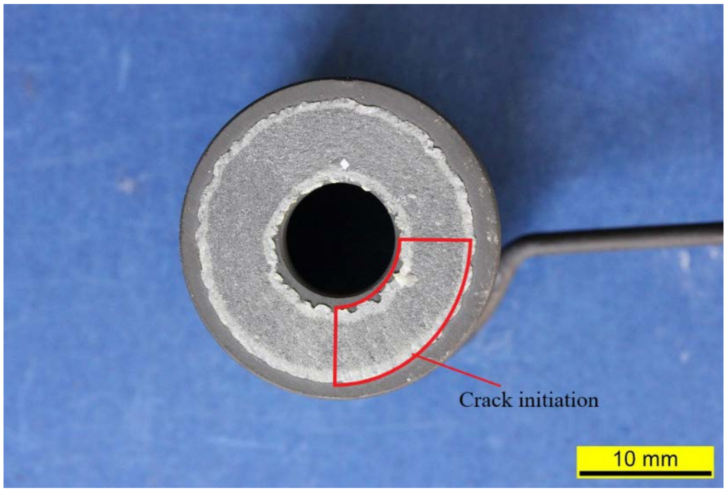

Fig. 15. Butt joint after tensile test.

Careful inspection of the specimen allows the lines of cracks formed in the quadrant enclosed by the solid line to be distinguished. Therefore, combining this with the previous analysis, it can be inferred that the crack began in a pore in this zone, or in any of the defects of the material, and once these became saturated because of the redistribution of internal stress fields, the debonding of the fracture surfaces began, without there being any breakage of fibers or crystals, but rather the pull-out of fibers and crystals from the matrix (i.e., the base of glass H).

4. Discussion

In the previous sections, a detailed acoustic emission analysis was carried out to define the fracture mechanisms of a glass ceramic composite, commonly required in the hermetic sealing of planar solid oxide cells under tensile loads. The experiments were carried out at room temperature.

As is shown above, data discrimination based on signal duration and amplitude made it possible to focus only on those signals with information relevant to the analysis, as well as facilitating data management. However, it is apparent that valuable information was omitted during the filtering process. An important finding is the fact that the events in cluster III, the transient signals, showed a linear trend that coincides with that previously proposed by [38].

On the other hand, the correlation of the amplitude of the events and stress load with time, as is shown in Fig. 4, made it clear that from the beginning of the application of the tensile load acoustic activity probably appeared due to the attraction forces generated between the different crystals, fibers and glass phase in the H-glass, i.e., the distribution of stresses in the internal planes of the ceramic glass. An important finding was of a stress saturation zone, probably in the pores or defects, towards the end of the test, which created a region with no acoustic activity. An implication of this behavior, in accordance with the fracture theory in ceramics [47], is that when these stress concentration points become saturated, they cannot find a way to alleviate this energy, as some ceramics exhibit small plastic zones and can release the energy, as a result, these become potential fracture nuclei. In addition, it is important to recall that there were also residual thermal stresses generated during the cooling process of the glass ceramic.

Parametric analysis based on signal amplitude shed light on AE waveforms but it was not possible to attribute these to any AE source event, as there were no previously published works to serve as a reference. Similarly, the application of the modal acoustic emission was not satisfactory because in this specific case rod waveguides were used that avoided the application of plate wave theory [41-43]. However, it was interesting to find that the wave mode that governed the experiments was the rod mode. This is because the wave of the propagated signal is transformed into the guided wave modes of the waveguide geometry [38].

As far as the frequency analysis is concerned, it can be noted that the frequency ranges found in this work fell within the frequency range considered in the current literature as an appropriate range, namely 10 to 550 kHz, for the analysis of glass fiber reinforced composite materials [50]. Accordingly, it was found that the dominant frequencies, in the first two examples, were in the range of 0-200 kHz, followed by others with lesser magnitude in the range of 200-400 kHz. Both were considered low frequency, but it was possible to attribute them to the debonding mechanism, which relates to the perpendicular separation of the fracture surfaces through the action of tensile loading. As explained above, this debonding could have occurred between the YSZ fibers and matrix, without breaking the fibers, which is known as fiber pull-out [51]. Also, however, the breaking of the H-glass could have occurred, i.e., matrix cracking. However, it was not possible to define which frequency is related to each of them.

The information shown in Fig. 11 was highly interesting, as it was an event that occurred within the limit of the glass ceramic sealant, whose maximum recorded load was 11 kN. The frequency spectra in this specific case showed a large number of peaks across the entire range under consideration. Of particular interest were those above 400 kHz, which were not observed in the two previous examples. This was a clear finding of another fracture mechanism known as fiber breakage, a result that coincided with that observed by other researchers [44-46]. It made sense because it was an event that occurred prior to the failure.

By means of a SEM/EDS analysis, it was known that the glass ceramic sealant was constituted of a matrix of glass H reinforced with YSZ fibers and some residual glass phases, which facilitated the interpretation of the results.

On the other hand, the hypotheses arising from the above results were tested by means of a visualization test carried out on one of the fracture surfaces of the specimen. Most importantly, possible crack paths were found on the surface where the possible initiation of the fracture was assumed. In this sense, the microstructure of the material was a key part in explaining what happened inside the ceramic glass during the test. The observed findings are supported by the theory of failure in glass ceramics [47].

Ultimately, it is important to note that in this experiment it was not possible to assign a particular frequency to each of the microscopic failure mechanisms found here: matrix cracking (i.e., glass H cracking), debonding and fiber pull-out (i.e., between glass H and YSZ fibers or crystals) and YSZ fiber breakage.

5. Conclusions

The experiments conducted in this study demonstrated the promising application of the acoustic emission technique for the monitoring of the mechanical degradation of planar SOC stacks. Special emphasis has been given to the glass ceramic composite material frequently used as a seal between the individual cells of SOC stacks.

Compared to other methods of noise signal discrimination, the method based on AE signal duration has proven to be simple and quick to apply. However, it has been found that its major drawback was the assignment of a criterion to determine the duration values that would allow a distinction between low and high durations.

In addition, the effect of the use of waveguides on the identification of possible wave modes was demonstrated. Therefore, an important contribution to the topic has been the discovery that in these experiments, the predominant wave mode was the rod mode.

On the other hand, the use of the FFT technique allowed for calculation of the frequency spectra in each of the examples considered here. Therefore, based on the results of previous research, the main contributions were a) for a frequency range from 50 to 400 kHz, having found that at 27% and 54% of the application of the tensile load the possible fracture mechanisms are present, considering the type of material and test, were the debonding and pull-out of the fibers, as well as some of the crystals from the H-glass surface and the cracking of glass H; and b) for frequencies higher than 400 kHz, the microscopic fracture mechanism identified was that of the breakage of the YSZ fibers or some of the crystals found in the composite material.

Finally, although it was not possible to assign specific frequencies to each of the fracture mechanisms present in these experiments, the results provide valuable information for understanding the fracture mechanism in the type of material used here. Therefore, it is recommended to develop more experiments supported by other techniques such as FEM modeling or electromagnetic emission.

Acknowledgements

The authors would like to express their gratitude for the contribution of colleagues from the different institutes of the Forschungszentrum Jülich, who provided valuable ideas, knowledge and information to complete this project. Special thanks to Ro. Peters (IEK-14), S.M. Gross-Barsnick (ZEA-1), D. Federmann (ZEA-1), M. Fischer (ZEA-1), A. Cramer (ZEA-1) and D. Mack (IEK-1). Special thanks goes to the valuable suggestions and comments made by M.G.R. Sause. Finally, many thanks to the University of Guanajuato for the sabbatical stay granted during the period 2019-2020.

References

[1] E. Miller, S. Thompson, K. Randolph, Z. Hulvey, N. Rustagi & S. Satyapal. US Deparment of Energy hydrogen and fuel cell technologies perspectives. *MRS Bulletin*. 2020:45:57-64. DOI:10.1557/mrs.2019.312.

[2] A.L. Dicks, D.A.J. Rand. Fuel cell systems explained. 3rd ed. New Jersey: Wiley; 2018.

[3] Q. Fang, L. Blum, R. Peters, M. Peksen, P. Batfalsky, D. Stolten. SOFC stack performance under high fuel utilization. Int J Hydrogen Energy. 2015:40:1128-36. https://doi.org/10.1016/j.ijhydene.2014.11.094.

[4] J. Malzbender, R.W. Steinbrech. Advanced measurement techniques to characterize thermo-mechanical aspects of solid oxide fuel cells. J Power Sources. 2007: 173:60-67. https://doi.org/10.1016/j.jpowsour.2007.07.072.

[5] L. Blum, S.M. Groß, J. Malzbender, U. Pabst, M. Peksen, R. Peters, I.C. Vinke. Investigation of solid oxide fuel cell sealing behaviour under stack relevant conditions at Forschungszentrum Jülich. J Power Sources. 2011:196:7175-7181.

[6] V. Subotic, S. Pofahl, V. Lawlor, N.H. Menzler, T. Thaller, C. Hochenauer. Online monitoring tools for SoH diagnostic and prognostic of remaining lifetime of reversible solid oxide cell (rSOC) systems. Energy Procedia. 2019:158:2329-2334. https://10.1016/j.egypro.2019.01.271.

[7] Y. Zhao, J. Malzbender. Elevated temperature effects on the mechanical properties of solid oxide fuel cell sealing materials. J Power Sources. 2013:239:500-504.

[8] Y. Zhao, J. Malzbender, S.M. Groß. The effect of room temperature and high temperature exposure on the elastic modulus, hardness and fracture toughness of glass ceramic sealants for solid oxide fuel cells. J Eur Ceram Soc. 2011:31:541-548.

[9] N. Lahl, K. Singh, L. Singheiser, K. Hilpert, D. Bahadur. Crystallisation kinetics in AO-Al2O3-SiO2-B2O3 glasses (A = Ba, Ca, Mg). J Mater Sci. 2000:35:3089-3096.

[10] J. Wei, G. Pecanac, J. Malzbender. Review of mechanical characterization methods f ceramics used in energy technologies. Ceramics International. 2014:40:15371-15380.

[11] F. Smeacetto, M. Salvo, M. Santarrelli, P. Leone, G.A. Ortigoza-Villalba, A. Lanzini, L.C. Ajitdoss, M. Ferraris. Perfromance of a glass-ceramic sealant in a SOFC short stack. Int J Hydrogen Energ. 2013:38:588-596. https://doi.org/10.1016/j.ijhydene.2012.07.025.

[12] A. Goel, M.J. Pascual, J.M.F. Ferreira. Stable glass-ceramic sealants for solid oxide fuel cells: influence of Bi_2O_3 doping. Int J Hydrogen Energ. 2010:35:6911-6923. https://doi.org/10.1016/j.ijhydene.2010.04.106.

[13] J. Malzbender, Y. Zhao, T. Beck. Fracture and creep of glass-ceramic solid oxide fuel cell sealant materials. J Power Sources. 2014:246:574-580.

[14] S.M. Gross, D. Federmann, J. Remmel, M. Pap. Reinforced composite sealants for solid oxide fuel cell applications. J Power Sources. 2011:196:7338-7342. https://doi.org/10.1016/j.jpowsour.2011.02.002.

[15] W. Zhang, X. Wang, Y. Dong, J. Yang, J. Pu, Bo Chi, Li Jian. Development of flexible ceramic-glass seals for intermediate temperature planar solid oxide fuel cell. Int J Hydrogen Energ. 2016:41:6036-6044. https://doi.org/10.1016/j.ijhydene.2016.02.120.

[16] B.Timurkutluk, T. Altan, S. Celik, C. Timurkutluk, Y. palace. Glass fiber reinforced sealants for solid oxide fuel cells. Int J Hydrogen Energ. 2019:44:18308-18318.

[17] G. Quinn. Strength and Proof testing, ASM International, Engineering Materials Handbook, 1991.

[18] Y. Zhao, Y. Zhao. Thermomechanical properties of glass-ceramic solid oxide fuel cell sealant materials. In: RWTH Aachen, 2013.

[19] J.W. Hutchinson. Mechanisms of toughening in ceramics, IUTAM, 1989.

[20] J. Wei. Mechanical characterization of solid oxide fuel cells and sealants. Energies & Umwelt/Energy & Environment. Forschungszentrum Jülich. 2017:391. ISBN: 978-3-95806-266-5.

[21] T. Shiotani, S. Yuyama, Z.W. Li, M. Ohtsu. Application of AE improved b-value to quantitative evaluation of fracture process in concrete materials. J Acoustic Emission. 2001:19:118-133.

[22] M.A. Rasheed, S.S. Prakash, G. Raju, Y. Kawasaki. Fracture studies on synthetic fiber reinforced cellular using acoustic emission technique. Const. Build. Mater. 2018:169:100-112. https:/doi.org/10.1016/j.conbuidmat.2018.02.157.

[23] J. McCrory. Advanced acoustic emission (AE) monitoring techniques for aerospace structures. PhD Thesis, Cardiff University.

[24] K.M. Holford, R. Pullin, S.L. Evans, M.J. Eaton, J. Hensman, K. Worden. Acoustic emission for monitoring aircraft structures. Proc. IMechE Vol. 223 Part G: J. Aerospace Engineering. 2009:223:525-532. https://doi.org/10.1243/09544100JAERO404.

[25] P. Rodriguez, T.B. Celestino. Application of acoustic emission and signal analysis to qualitative and quantitative characterization of the fracturing process in rocks. Eng Frac Mech. 2019:210:54-69. https://doi.org/10.1016/j.engfracmech.2018.06.027.

[26] Z. Ge, Q. Sun. Acoustic emissions (AE) characteristics of granite after heating and cooling cycles. Eng frac Mech. 2018:200:418-419. https://doi.org/10.1016/j.engfracmech.2018.08.011.

[27] C.S. Kumar, V. Arumugam, R. Sengottuvelusamy, S. Srinivasan, H.N. Dhakal. Failure strength prediction of glass/epoxy composite laminates from acoustic emission parameters using artificial neural network. Appl Acoustics. 2017:115:32-41. https://doi.org/10.1016/j.apacoust.2016.08.013.

[28] A. Yonezu, X. Chen. Micro-scale damage characterization in porous ceramics by an acoustic emission technique. Ceramics. 2014:40:9859-66. https//doi.org/10.1016/j.ceramint.2014.02.079.

[29] M. Surgeon, E. Vanswijgenhoven, M. Wevers, O. Van Der Biest. Acoustic emission during tensile testing of SiC-fibre-reinforced BMAS glass-ceramic composites. Compos Part A. 1997:28A:473-480.

[30] W.K. Jiayu Li, S. Liu, Z. Lin. The influence of interconnect ribs on the performance of planar solid oxide fuel cell and formulae for optimal rib sizes. J Power Sources. 2012:204:106-15.

[31] K. Sato, K. Omura, T. Hashida, K. Yashiro, H. Yugami, T. Kawada, J. Mizusaki. Tracking the onset of damage mechanism in ceria-based solid oxide fuel cells under simulated operating conditions. J Test Eval. 2006:34:246-250.

[32] S. M. Gross, T. Koppitz, J. Remmel, J.B. Bouche, U. Reisgen. Joining properties of a composite glass-ceramic sealant. Fuel Cells Bulletin. 2006:9:12-15. Doi:10.106/S1464-285(06)71320-7.

[33] S.M. Gross, C. Babelot, D. Federmann, U. Pabst. Optimization of tensile strength measurements on glass-ceramic sealant used for SOFC stacks. ECS Transactions. 2015:68(1):2573-2582.

[34] B.C. Greven, S.M. Gross-Barsnick, T. Koppitz, R. Conradt, F. Smeacetto, A. Ventrella, M. Ferraris. Torsional shear strength of novel glass-ceramic composite sealant for solid oxide fuel cell stacks. Int J Appl Cream Technol. 2018:15:286-295. https://doi.org/10.1111/ijac.12819.

[35] Vallen Systeme GmbH. 2017.

[36] Matlab 8.0 The Mathworks, Inc. Natick, Massachusetts, United States.

[37] N.N. Hsu, F.R. Breckenridge. Characterization and calibration of acoustic emission sensors. Mater Eval. 1981:39:60-68.

[38] M.G.R. Sause. In situ monitoring of fiber-reinforced composites: theory, basic concepts, methods and applications. Springer Int. Publishing. Switzerland. Doi: 10.1007/978-3-319-30954-5.

[39] A. R. Oskouei, H. Heidary, M. Ahmadi, M. Farajpur. Unsupervised acoustic emission data clustering for the analysis of damage mechanisms in glass/polyester composites. Materials and Designs. 2012:37:416-422. DOI:10.1016/j.matdes.2012.01.018.

[40] W.H. Prosser, K.E. S. Kellas, B.T. Smith, J. McKeon, A. Friedman. Advanced, waveform, based acoustic emission detection of matrix cracking in composites. Mater Eval. 1995:53:1052-1058.

[41] C.U. Grosse, M. Ohtsu. Acoustic emission testing. Springer. Berlin, 2018.

[42] J.J. Scholey, P.D. Wilcox, M.R. Wisnom MR, M.I. Friswell. Quantitative experimental measurements of matrix cracking and delamination using acoustic emission. Compos. Part A. Appl. Sci. manuf. 2010:41:612-623. Doi:10.1016/j.compositesa.2010.01.008.

[43] M. Surgeon, Wevers M. Modal analysis of acoustic emission signals from CFRP laminates. NDT E Int. 1999:32:311-322.

[44] A. Gupta, J.C. Duke Jr. Identifying the arrival of extensional and flexural wave modes using wavelet decomposition of ultrasonic signals. Ultrasonics. 2018:82:261-271. Doi:10.1016/j.ultras.2017.09.008.

[45] C.R. Ramirez-Jimenez, N. Papadakis, N. Reynolds, T.H. Gan, P. Purnell, M. Pharaoh. Identification of failure modes in glass/polypropylene composites by means of the primary frequency content of the acoustic emission event. Compos. Sci. Technol. 2004:64:1819-1827. Doi:10.1016/j.composcitech.2004.01.008.

[46] L. Yang, T.T. Yang, Y.C. Zhou, Y.G. Wei, R.T. Wu, N.G. Wang. Acoustic emission monitoring and damage mode discrimination of APS thermal barrier coatings under high temperature CMAS corrosion. Surf. Coat. Technol. 2016:304:272-282. DOI:10.1016/j.surfcoat.2016.06.080.

[47] A. Marec, J.H. Thomas, R. Gouerjoma. Damage characterization of polymer-based composite materials: multivariable analysis and wavelet transform for clustering acoustic emission data. Mech. Syst. Signal Process. 2008:22:1441-1464. Doi:10.1016/j.ymssp.2007.11.029.

[48] S.M. Wiederhorn. Fracture of ceramics. In: Mechanical and thermal properties of ceramics (ed. Watchman, J.B.Jr.). NBS Special Publication.1969:303:217-242.

[49] J. Brendt, S.M. Gross, C. Babelot, G. Natour. The influence of ZnO and V2O5 on the crystallization behavior of BaO-CaO-SiO2 glass ceramic sealants. J Non Cryst Solids. 2018:501:78-84. https://doi.org/10.1016/j.jnoncrysol.2018.01.032.

[50] G. Qi, Wavelet-based AE characterization of composite materials. NDT & I. 2000:33:136.

[51] M.G.R. Sause, A. Gribov, A.R. Unwin, S. Horn. Pattern recognition approach to identify natural clusters of acoustic emission signals. Pattern Recognition Letters. 2012:33:17-23. Doi:10.1016/j.patrec.2011.09.018.